Doppler and Pseudorange Measurements as Prediction Features for Multi-Constellation GNSS LoS/NLoS Signal Classification

Jasmine Zidan
WMG
The University of Warwick
Coventry, UK
j.zidan@warwick.ac.uk

Esther Anyaegbu
Spirent Communications Plc
Daventry, UK
esther.anyaegbu@spirent.com

Erik Kampert
Institute of Fundamentals of Electrical Engineering
Helmut-Schmidt-University
Hamburg, Germany
erik.kampert@hsu-hh.de

Matthew D. Higgins
WMG
The University of Warwick
Coventry, UK
m.higgins@warwick.ac.uk

Colin Ford
Spirent Communications Plc
Paignton, UK
colin.ford@spirent.com

***Abstract*—Precise positioning and timing are key challenges for safety & security critical applications in autonomous and trusted vehicles (ATVs). A global navigation satellite system (GNSS) receiver is one of the sensors used in ATVs to provide a satellite-based positioning, navigation and timing solution. GNSS robustness in built-up areas like urban canyons and in sheltered locations like multi-storey car parks is severely impaired due to non-line-of-sight and multi-path signal propagation. In this paper, an optimised decision tree classifier is used for the discrimination of GNSS signals into line-of-sight and non-line-of-sight signals. In addition to using the carrier-to-noise ratio and the satellite elevation angle as prediction features, adding the pseudoranges and the Doppler measurements enhances the classifier performance by $12\,\%$. As a result, an overall prediction accuracy of $97.8\,\%$ is obtained. For the studied data-set, the pseudorange measurements have a higher prediction importance than the Doppler measurements. Also evaluated in this study, is the use of a GPS L1 signal prediction regression model on other GNSS constellations. Analysis of the investigated scenario shows that the use of the current model is not adequate for non-GPS constellations.**

***Index Terms*—Machine Learning, ATVs, GNSS, Positioning, Classification, precision**

The doctorate of J. Zidan is supported by Spirent Communications Plc.as part of the Warwick Collaborative Postgraduate Research Scholarships (WCPRS).

I. Introduction

Precise localization and timing in urban canyons is a key autonomous and trusted vehicle (ATV) challenge that needs addressing [1], [2]. The use of healthy, uncorrupted and reliable global navigation satellite system (GNSS) signals enhances the position estimation. Having previous knowledge or a prediction about GNSS signal availability, which is also known as GNSS foresight, might help in various applications, such as route planning and real-time decision-making, where ATV sensors can

temporarily take over GNSS without suffering system reliability issues. Hence, further understanding of GNSS signal classification methods is of great importance.

This study expands on previous GNSS signal classification studies [3], [4] with an investigation of additional predictor features and multi-constellation GNSS. It is structured as follows: the next sub-section introduces related work, sub-section I-B highlights the contribution of this paper, Section II then presents the antenna setup and GNSS data collection, Section III illustrates the ground truth and data labeling, Section IV presents the results and the discussion, and Section V concludes the paper and provides suggestions for future work.

A. Related Works

Numerous methods have been proposed to detect and mitigate GNSS multipath and non-line-of-sight (NLoS) effects. Methods at the antenna level, such as using an antenna array or multi-frequency antenna, are efficient interference mitigating methods [5], [6]. Techniques related to the receiver design and the advanced algorithms deployed at the receiver level, such as vector tracking [7], can also mitigate multipath effects. As for the navigation processor-based methods, such as 3D mapping and consistency checks, they are also widely used in the literature to label LoS/NLoS signals [8]–[10]. The labeled data can be used to aid machine learning (ML) algorithms based on the desired application [6]. The use of ML for GNSS has been presented in [3]

The common signal classification method is to define a C/N_o threshold where lower C/N_o values are classified as unhealthy signals [11]. Whereas C/N_o is a good predictor in an interference free environment, such as an open sky, it is not the case for urban canyons, as various parameters might affect the C/N_o value (e.g. constructive and destructive multipaths) [12]. Hence, further GNSS signal features are needed to enhance the classification performance. In [11] the authors proposed a gradient-boosting decision tree (DT) classification algorithm based on the satellite elevation angle, C/N_o and the pseudorange residuals as prediction features. Authors in [13] proposed a DT-based classifier to detect GNSS signals based on two features: the satellite elevation angle and the difference between the C/N_o provided by RHCP and LHCP antennas, respectively. Only GPS L1 data was considered for training the model.

In addition to the C/N_o and satellite elevation angles, this paper investigates the use of pseudoranges and the Doppler measurements for classifications. The novelty in this work is in both the evaluated prediction features as well as in optimising the proposed DT algorithm.

B. Contribution

In ATV applications, where the reliability of GNSS-based positioning, navigation and timing (PNT) system is essential, the misprediction of LoS signals as NLoS would result in poor location estimation. Moreover, the receiver might not obtain a position fix in dense urban canyons with limited satellite visibility. Furthermore, the misclassification of NLoS as LoS will introduce position errors to the estimated position, which is critical for accuracy-sensitive applications. Hence, a better understanding of classification models and their outcomes is necessary to avoid classification model fitting problems. This is particularly important in the case of over-fitting, which introduces high prediction accuracy that is falsely trusted by the satellite-vehicle system.

This study investigates the use of GNSS pseudoranges and Doppler measurements to aid in classifying multi-constellation GNSS signals into either LoS or NLoS. GNSS signals from GPS, Galileo, GLONASS and BeiDou are collected using a NovAtel high-precision antenna and receiver, and the extracted information from the logged data is used as a ground truth. A fine decision tree classification method is built based on four features, namely: signal strength, elevation angle, pseudorange and Doppler frequency shift. The results show that adding these features to the prediction method enhances its performance. The results are compared with DTs based on various feature combinations. This work also highlights that the relationship be-

Fig. 1. GNSS receiver placement in a sub-urban environment.

```
$GAGSV,1,1,04,12,52,213,50,11,43,300,49,04,39,247,49,27,16,066,*64
$GQGSV,1,1,00,,,,*78
$BDGSV,2,1,06,22,77,057,54,21,44,273,55,12,38,252,47,34,35,286,50*6D
$BDGSV,2,2,06,71,28,222,49,11,26,313,45*69
#CLOCKSTEERINGA,USB1,0,45.5,FINESTEERING,2112,73972.504,02044000,0f61,15
#TIMEA,USB1,0,45.5,FINESTEERING,2112,73973.000,02044000,9924,15826;VALID
$GPGSV,2,1,07,09,84,113,53,06,68,237,53,04,47,060,48,02,43,300,50*7B
$GPGSV,2,2,07,07,27,159,48,19,14,223,37,05,10,285,45*4D
#RANGEA,USB1,0,45.5,FINESTEERING,2112,73973.000,02044000,5103,15826;41,2
82716.059698,0.007,-110.773,53.2,79.964,1810bda4,9,0,20262985.712,0.080,
7,0.007,1602.473,52.7,71.814,02333d24,11,0,23784425.877,0.053,-124988001
324.078,51.5,67.438,10349fe4,21,0,23283358.566,0.013,-121242554.459215,0
#INSPVAXA,USB1,0,45.5,FINESTEERING,2112,73973.000,02044000,471d,15826;WA
#CLOCKMODELA,USB1,0,45.5,FINESTEERING,2112,73973.000,02044000,98f9,15826
#BESTGNSSPOSA,USB1,0,45.5,FINESTEERING,2112,73973.000,02044000,bede,1582
<BESTSATS USB1 0 45.5 FINESTEERING 2112 73973.000 02044000 be05 15826
<     24
<          GPS 2 GOOD 00000003
<          GPS 4 GOOD 00000003
<          GPS 5 GOOD 00000003
<          GPS 6 GOOD 00000003
<          GPS 7 GOOD 00000003
<          GPS 19 NOIONOCORR 00000000
<          GPS 9 GOOD 00000003
<          GLONASS 0-6 NOEPHEMERIS 00000000
```

Fig. 2. A sample of the raw GNSS receiver log file.

tween the C/N$_o$ and elevation angle, which applies to GPS L1 signals, is inadequate for generalisation to other satellite constellations.

II. Antenna Setup and GNSS Data Collection

A NovAtel VEXXIS® GNSS-800 series antenna is used to record multi-constellation GNSS data in an almost open-sky sub-urban area. Figure 1 shows the antenna's placement in the garden of a terrace house with an antenna height of $1.3\,\mathrm{m}$ and at $1.85\,\mathrm{m}$ distance from a $1.7\,\mathrm{m}$ high wooden fence. The antenna's National Marine Electronic Association (NMEA) data sentences, channel measurements for the currently tracked satellites (RANGEA log) and the BESTSATS log are received. To decode this received satellite information, a custom Python-based extractor/reader has been developed. A sample of the GNSS receiver log file is shown in Figure 2. Each line of these raw data is called a sentence and each observation is an independent self-contained sentence.

For the data analysis, only the GPS L1, GLONASS L1, Galileo E1 and BeiDou B1 signals are extracted from the RANGEA-log. The channel tracking status field (ch-tr-status) is first read and analysed, and the corresponding signal characteristics C/N$_o$, elevation, Doppler and pseudoranges are extracted from the RANGEA-log. Furthermore, the azimuth and the elevation angles are extracted from the GNSS satellite in view NMEA (GSV) log messages. Subsequently, MATLAB scripts are used to analyse and reprocess the data. In total, 100913 observations are obtained in this process, with the number of samples per individual constellation as follows: 33974 for BeiDou, 27010 for GPS, 22249 for GLONASS and 17707 for Galileo.

III. Ground Truth and Data Labeling

For data labeling, Deep et al. [14] derived a GPS signal C/N$_o$ correlation with the satellite vehicle'S (SV) elevation angle in an urban environment. The suggested threshold has been used in other literature to predict if a GPS signal is LoS or obscured, and is described by

$$C/N_o = 3.199\times10^{-5}\times\theta^3 - 0.0081\times\theta^2 + 0.6613\times\theta + 31.38 \quad (1)$$

where θ is the SV's elevation angle and C/N$_o$ is the predicted threshold correlated with the satellite elevation angle. Values smaller than the predicted C/N$_o$ indicate an obscured signal, whereas higher values are considered as LoS.

However, when evaluating the regression in Equation 1 on predicting signal classes from the Indian GNSS constellation NavIC, the results showed that it was not suitable [15]. Furthermore, the method has not been thoroughly investigated for other constellations. Hence, the use of the mathematical model described by Equation 1 to predict the signals of BeiDou, GPS, Galileo and GLONASS constellations individually, is further investigated first.

A. Evaluating the C/N$_o$ Prediction Regression Model

When comparing the regression performance with the *lock state* information derived from the installed high-precision antenna and receiver, the

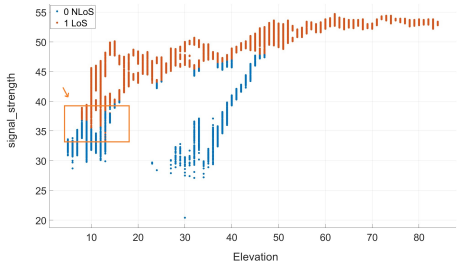

Fig. 3. Scatter plot of the GPS data based on the *lock state* information, with LoS and NLoS signals in red and blue, respectively.

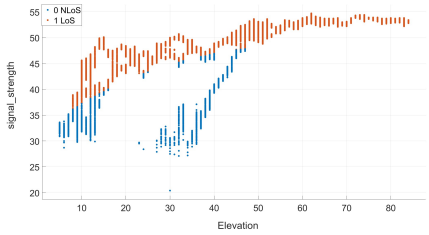

Fig. 4. Scatter plot of the predicted GPS data based on the regression model, with LoS and NLoS signals in red and blue, respectively.

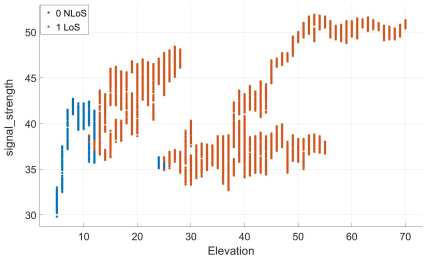

Fig. 5. Scatter plot of the GLONASS data based on the *lock state* information, with LoS and NLoS signals in red and blue, respectively.

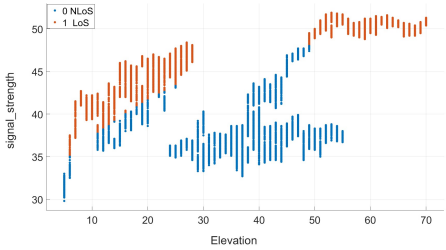

Fig. 6. Scatter plot of the predicted GLONASS data based on the regression model, with LoS and NLoS signals in red and blue, respectively.

regression's *goodness of fit* indeed works perfectly for the GPS constellation. In Figures 3 (*lock state*) and 4 (regression) the analysis of this GPS signal prediction is presented, with the LoS and NLoS signals in red and blue, respectively, and the area of disparity featured inside the orange box.

With regards to evaluating the *goodness of fit* for other constellations, it is clear from Figures 6 and 8 that the C/N_o-elevation angle correlation based on GPS L1 signals does not provide optimal results for predicting obscured signals for other constellations, as the model displays fitting issues especially for GLONASS and BeiDou, when compared to the receiver's *lock state* information in Figures 5 and 7, respectively. Figure 10 shows that based on the regression model, some of the Galileo signals with elevation angles smaller than 10° are considered as LoS. On the other hand, Galileo signals with relatively high elevation angles over 28° and at a C/N_o over $40\,\mathrm{dBm}$ are considered as NLoS. This observation does not hold for the *lock state* information provided in Figure 9.

This observed difference in regression performance between constellations can be due to the differences in the constellation design as the minimum received power and the frequencies vary among different constellations. The adopted orbits and the SVs' distribution affect the C/N_o-elevation correlation, elevation and the azimuth angles. For example, the BeiDou constellation is designed to transmit at lower signal strength levels than GPS. Moreover, whereas GPS satellites move in the medium earth orbit (MEO), BeiDou satellites adopt three orbits: geostationary orbit (GEO), MEO and the inclined geosynchronous orbit (IGSO) [16].

Further investigation with multiple data-sets is needed for a holistic evaluation of the use of the regression method underlying Equation 1 as a ground truth for LoS and NLoS labeling when used for multiple constellations. Hence, for the evaluation of the decision tree classification in this work, the receiver's logged *lock state* will be used

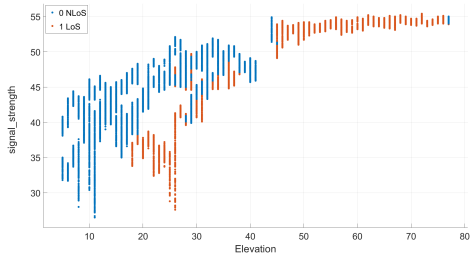

Fig. 7. Scatter plot of the BeiDou data based on the *lock state* information, with LoS and NLoS signals in red and blue, respectively.

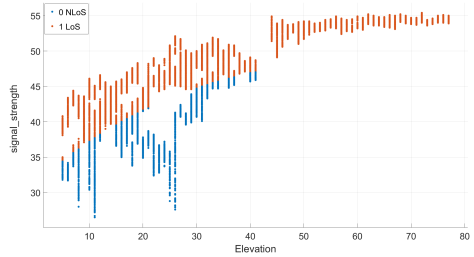

Fig. 8. Scatter plot of the predicted BeiDou data based on the regression model, with LoS and NLoS signals in red and blue, respectively.

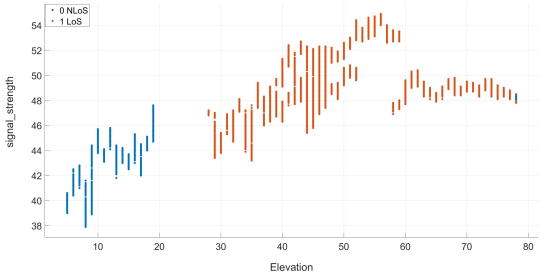

Fig. 9. Scatter plot of the Galileo data based on the *lock state* information, with LoS and NLoS signals in red and blue, respectively.

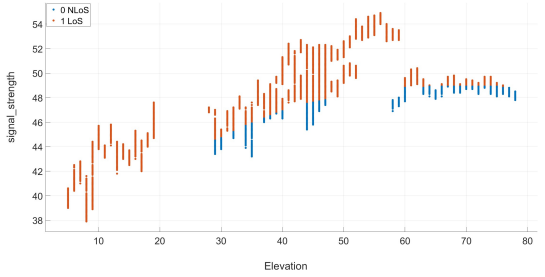

Fig. 10. Scatter plot of the predicted Galileo data based on the regression model, with LoS and NLoS signals in red and blue, respectively.

as the ground truth.

B. Two-step Labeling

The results presented in the previous section have shown that the investigated regression is not adequate to be used in the case of constellations other than GPS. Therefore, a two-step labeling process is proposed instead: the first labeling criterion depends on the messages from the receiver logs and the second criterion depends on the geometrical boundaries of buildings and structures in the receiver's surrounding environment. For the first labeling step, the *lock state* is extracted from the receiver's BESTSATS-log as a ground truth. BESTSATS lists the *lock state* of both used and unused satellite signals for estimating the corresponding position solution. The *lock state* in this specific data-set provides eight different categories, which are displayed in Figure 11. Following the BESTSATS-log nomenclature, observations in the category 'Good' are used in the positioning solution and have a strong likelihood to be healthy LoS signals. Therefore, in Figure 11 those signals are labeled as LoS and presented as red dots. Observations with a *lock state* other than 'Supplementary' or 'Good' are excluded from the positioning solution, as they represent unhealthy, obscured signals. These signals are labeled as NLoS and presented in blue in Figure 11. Although some of the observations that are in the 'Supplementary' *lock state* can be used by the NovAtel receiver for estimating the positioning solution, these data could either be obscured or healthy signals. One of the reasons for the receiver not to use the healthy 'Supplementary' signals might be the geometry of the satellites in the sky. If the satellites are clustered, the estimated position might have a lower precision. These signals are labeled as 'Supplementary' and presented in yellow in Figure 11.

In the second labeling step, in addition to the BESTSATS log, a minimum elevation angle thresh-

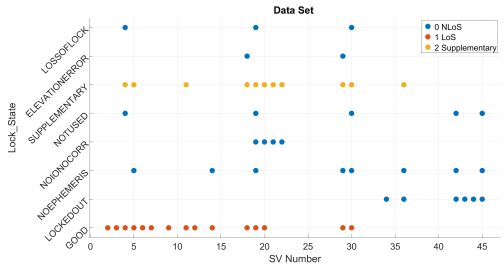

Fig. 11. Data labeling based on the *lock state*.

old is applied. This threshold is calculated as follows:

$$\theta = tan^{-1}(h \setminus d) \tag{2}$$

in which θ is the elevation angle threshold for satellite visibility, h is the height of the obstacle (in this case a building or structure) minus the height of the antenna in metres, and d is the distance between the object and the antenna in metres. This step is required to define observations with the 'Supplementary' label as either LoS or NLoS. Moreover, a more accurate ground truth can be achieved, as applying this step will exclude any multi-path signals from observations with a 'Good' *lock state*, that were previously labeled as LoS in the first labeling step. Table I describes the labeling of the satellite signals with the 'Supplementary' *lock state* in more detail. The data labels adopted are label '1' for LoS data and label '0' for data representing multipath or NLoS signals.

Figure 12 represents an exemplary sky-plot that displays the SVs visible in the sky at a certain time of the day with the buildings and structures surrounding the receiver as a background image. As an example of SV visibility, the minimum and maximum elevation angle for SV GPS 4 in Table I is $21°$ and $67°$, respectively. SV GPS 4 is represented as 4* in Figure 12 and requires a minimum elevation angle of $45.5°$ to be in direct visibility of the antenna without obscuration by its surroundings. Therefore, in Table I, observations with elevation angles smaller than this specific elevation threshold are labelled as '0' and observations above the threshold are labelled as '1'.

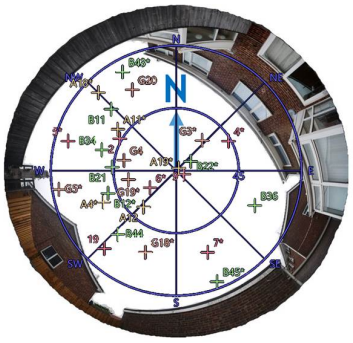

Fig. 12. Satelite vehicles' sky visibility.

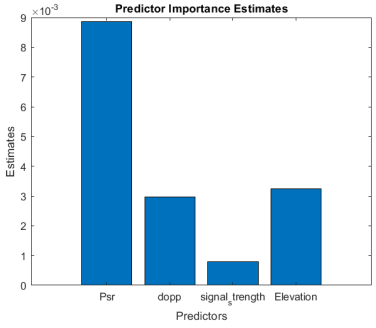

Fig. 13. Predictor importance estimates.

IV. Results and Discussion

Performing the decision tree classification method on the data-set shows the effect of different characteristic signal features on the algorithm's accuracy. The accuracy characterizes the performance of the algorithm with $70\,\%$ of the chronologically randomized data-set used for training and $30\,\%$ used for testing. The main objective of this study is to investigate the use of pseudoranges and Doppler measurements as predictors on the performance of the DT. Results for this specific scenario and data-set show that adding the pseudoranges as a predictor enhances the prediction accuracy by $12\,\%$ compared to when only using the signal strength and the elevation angle as predictors. With respect to the Doppler feature, the determined overall prediction accuracy of the fine decision tree is $89.7\,\%$ for both the training and testing data-sets. This

TABLE I
SATELLITE VEHICLES WITH A 'SUPPLEMENTARY' LOCK STATE

constellation	BeiDou		GPS					GLONASS					Galileo		
SV Number	*B21*	*B22*	*4*		*19*	*29*	*30*	*G4*	*G5*	*G18*		*G20*	*A11*	*A19*	*A36*
C/N_0	*51-53*	*54.5*	*43-48*	*30-42*	*32*	*35*	*31-34*	*50*	*37.6*	*31*	*45*	*35.4*	*49.7*	*48*	*45*
Elevation (Min-Max) in $^\circ$	*45-67*	*55-77*	*46-67*	*21-45*	*5-13*	*8*	*9-13*	*45-70*	*11*	*5-12*	*13-27*	*24-25*	*46*	*78*	*5-19*
Elevation threshold in $^\circ$	*12*	*46*	*46*	*46*	*13*	*14*	*14*	*13*	*12*	*13*	*13*	*13*	*12*	*46*	*13*
Label	*1*	*1*	*1*	*0*	*0*	*0*	*0*	*1*	*0*	*0*	*1*	*1*	*1*	*1*	*0*

Fig. 14. Analysis of the decision tree model with four predictors.

feature enhances the algorithm's accuracy by $5\,\%$. Table II presents the feature selection and corresponding prediction accuracy for the DT. It can be noticed that a $97.8\,\%$ prediction accuracy can be achieved when using four prediction features.

The predictor importance of the used features can be computed by summing the changes in the node risk due to splits at every subsequent predictor, divided by the number of the branches. In Figure 13 the predictor importance estimates are represented. The pseudorange has the highest predictor importance for this data-set. In contrast, the signal strength has the least significance, whereas the Doppler measurements only have a slightly lower effect on the prediction when compared to the elevation angle. Therefore, Figure 13 corresponds to the obtained model accuracy outcome. Adding pseudorange as a predictor has introduced the most significant enhancement to the DT compared with the Doppler measurement and elevation angle.

To avoid over-fitting the trained model, the DT-depth has been evaluated and the maximum splitting number is set to 24 splits. In Figure 14 the confusion matrix of the DT model is presented. Figure 14a shows that 1343 observations are classified as LoS, although their actual class is NLoS. Figure 14b and Figure 14c show that approximately $7\,\%$ of the total NLoS observations is misclassified, which represent $2.6\,\%$ of the entire training data-set. This misclassification might be due to using the same predictor thresholds to classify observations from different GNSS constellations.

TABLE II
FEATURE SELECTION AND CORRESPONDING PREDICTION ACCURACY FOR A DEPTH-CONTROLLED FINE DECISION TREE.

Features used in Prediction	Validation	Testing
C/N_0 and Elevation	$84\,\%$	$84\,\%$
C/N_0 , Elevation , Doppler	$89.7\,\%$	$89.7\,\%$
C/N_0 , Elevation , Psr	$96\,\%$	$96\,\%$
C/N_0 , Elevation, Doppler, Psr	$97.8\,\%$	$97.9\,\%$

V. Conclusion & Future work

The presented work has been carried out to study the impact of GNSS pseudoranges and the Doppler-effect on classifying received GNSS signals as LoS or obscured/NLoS signals. The presented analysis for the specific sub-urban experimental setting shows that both pseudoranges and Doppler can enhance the classification if added as classification features. The developed decision tree classification model shows that the pseudorange has a higher importance as a classifying feature than the Doppler effect. The enhancement in the prediction accuracy is up to $13\,\%$ when compared to using the signal strength and the elevation angle as standalone features.

In this work, a static GNSS receiver in one location has been investigated as a proof of concept. The presented methodology can be further developed to include measurements from different times of the day and additional locations, as well as on a moving vehicle. Furthermore, the algorithms as well as additional GNSS data recorded using a commercial antenna could be used to further evaluate the presented methodology.

Acknowledgment

The authors would like to acknowledge the efforts of Ronald Wong in providing the recorded data.

References

[1] Government Office for Science, "Satellite-derived Time and Position: A Study of Critical Dependencies 2 Satellite-derived Time and Position," *Government Office for Science*, pp. 1–86, 2018. [Online]. Available: https://bit.ly/2NtRcj4

[2] S. Srinara, S. Tsai, C.-X. Lin, M.-L. Tsai, and K.-W. Chiang, "Reliable Evaluation of Navigation States Estimation for Automated Driving Systems," in *2022 IEEE Intelligent Vehicles Symposium (IV)*, 2022, pp. 1765–1773.

[3] E. I. Adegoke, J. Zidane, E. Kampert, P. A. Jennings, C. R. Ford, S. A. Birrell, and M. D. Higgins, "Evaluating Machine Learning & Antenna Placement for Enhanced GNSS Accuracy for CAVs," in *2019 IEEE Intelligent Vehicles Symposium (IV)*, 2019, pp. 1007–1012.

[4] J. Zidan, O. Alluhaibi, E. I. Adegoke, E. Kampert, M. D. Higgins, and C. R. Ford, "3D Mapping Methods and Consistency Checks to Exclude GNSS Multipath/NLOS Effects," in *2020 International Conference on UK-China Emerging Technologies (UCET)*, 2020, pp. 1–4.

[5] Z. Jiang and P. D. Groves, "NLOS GPS Signal Detection Using a Dual-Polarisation Antenna," *GPS Solutions*, vol. 18, no. 1, pp. 15–26, 2014.

[6] S. Ollander, F. A. Schiegg, F.-W. Bode, and M. Baum, "Dual-frequency Collaborative Positioning for Minimization of GNSS Errors in Urban Canyons," in *2020 IEEE 23rd International Conference on Information Fusion (FUSION)*, 2020, pp. 1–8.

[7] L.-T. Hsu, S.-S. Jan, P. D. Groves, and N. Kubo, "Multipath Mitigation and NLOS Detection Using Vector Tracking in Urban Environments," *GPS Solutions*, vol. 19, pp. 249–262, 2015. [Online]. Available: https://link.springer.com/content/pdf/10.1007%2Fs10291-014-0384-6.pdf

[8] M. Adjrad and P. D. Groves, "Intelligent Urban Positioning: Integration of Shadow Matching with 3D-Mapping-Aided GNSS Ranging," *Journal of Navigation*, vol. 71, no. 1, pp. 1–20, 2018.

[9] L. T. Hsu, H. Tokura, N. Kubo, Y. Gu, and S. Kamijo, "Multiple Faulty GNSS Measurement Exclusion Based on Consistency Check in Urban Canyons," *IEEE Sensors Journal*, vol. 17, no. 6, pp. 1909–1917, 2017.

[10] L. Hsu, "GNSS Multipath Detection Using a Machine Learning Approach," in *2017 IEEE 20th International Conference on Intelligent Transportation Systems (ITSC)*, Oct 2017, pp. 1–6.

[11] R. Sun, G. Wang, W. Zhang, L.-T. Hsu, and W. Y. Ochieng, "A Gradient Boosting Decision Tree Based GPS Signal Reception Classification Algorithm," *Applied Soft Computing*, vol. 86, p. 105942, 2020.

[12] R. Yozevitch, B. B. Moshe, and A. Weissman, "A Robust GNSS LOS/NLOS Signal Classifier," *Navigation: Journal of The Institute of Navigation*, vol. 63, no. 4, pp. 429–442, 2016.

[13] B. Guermah, H. E. Ghazi, T. Sadiki, and H. Guermah, "A Robust GNSS LOS/Multipath Signal Classifier based on the Fusion of Information and Machine Learning for Intelligent Transportation Systems," in *2018 IEEE International Conference on Technology Management, Operations and Decisions (ICTMOD)*, 2018, pp. 94–100.

[14] S. Deep, S. Raghavendra, and B. Bharath, "GPS SNR Prediction in Urban Environment," *The Egyptian Journal of Remote Sensing and Space Science*, vol. 21, no. 1, pp. 83–85, 2018.

[15] V. Chamoli, R. Prakash, and A. Vidyarthi, "Mathematical Regression Model to predict Navigation with Indian Constellation (NavIC) Geo Synchronous Satellite System," in *2020 Global Conference on Wireless and Optical Technologies (GCWOT)*, 2020, pp. 1–5.

[16] X. Ma, K. Yu, X. He, J.-P. Montillet, and Q. Li, "Positioning Performance Comparison between GPS and BDS with Data Recorded at four MGEX Stations," *IEEE Access*, vol. 8, pp. 147 422–147 438, 2020.